ISSN 2278-2540 | DOI: 10.51583/IJLTEMAS | Volume XV, Issue VII, July 2026

Enhanced Upconversion Luminescence and Physical Characteristics of Ho^{3+}-Doped Tungsten Tellurite Glasses for Photonic Applications

Smriti Tiwari., Ghizal F. Ansari*

Department of Physics, Madhyanchal Professional University, Bhopal, India

***Corresponding Author**

DOI: https://doi.org/10.51583/IJLTEMAS.2026.150700143

Received: 13 August 2026; Accepted: 18 August 2026; Published: 24 August 2026

ABSTRACT

Holmium (Ho^{3+})-doped tungsten tellurite glasses with the composition $(70-x)TeO_2–10Na_2O–20WO_3–xHo_2O_3$ (x = 0.5–1.5 mol%) were successfully synthesized using the conventional melt-quenching technique to investigate their suitability for visible upconversion and photonic applications. X-ray diffraction analysis confirmed the amorphous nature of all prepared samples, while differential scanning calorimetry demonstrated good thermal stability with a glass transition temperature of approximately 310 °C and a crystallization temperature near 500 °C. Various physical parameters, including density, molar volume, lanthanide ion concentration, polaron radius, interionic distance, field strength, and oxygen packing density, were evaluated to understand the structural modifications induced by Ho^{3+} incorporation. The density and lanthanide ion concentration increased systematically with increasing Ho^{3+} content, whereas the molar volume, interionic distance, and polaron radius decreased, indicating progressive densification and strengthening of the glass network. Optical absorption spectra exhibited characteristic Ho^{3+} transitions in the visible and near-infrared regions, confirming efficient incorporation of rare-earth ions into the tellurite glass matrix. Under 980 nm laser excitation, intense upconversion emissions centered at approximately 547 nm (green), 660 nm (red), and 760 nm (near-infrared) were observed, corresponding to the $^5F_4/^5S_2 \rightarrow {}^5I_8$, $^5F_5 \rightarrow {}^5I_8$, and $^5S_2 \rightarrow {}^5I_7$ transitions of Ho^{3+} ions, respectively. The emission intensity increased with excitation power, demonstrating efficient excited-state absorption and cross-relaxation processes responsible for the observed upconversion mechanism. The combination of favorable thermal stability, enhanced physical characteristics, and strong visible upconversion emission demonstrates that Ho^{3+}-activated tungsten tellurite glasses are promising candidates for solid-state lasers, optical amplifiers, color display devices, and other advanced photonic applications.

Keywords: Tellurite glass; Ho^{3+} ions; Upconversion luminescence; Melt-quenching; Rare-earth-doped glasses; Photonic materials; Optical spectroscopy.

INTRODUCTION

Glasses have emerged as superior host materials for optically active ions, primarily because they offer a unique combination of thermal and chemical resilience. Their ability to be manufactured in both fiber and bulk configurations, coupled with recyclability and optical transparency, makes them ideal candidates for photonic applications. A key advantage lies in their amorphous structure—the lack of long-range crystalline order creates multiple emissive sites for activator ions, enabling fine-tuning of luminescent properties [1]. This structural flexibility has made glassy systems increasingly attractive for developing advanced opto-electronic and photonic technologies, particularly in optical sensing and thermal monitoring applications [2–7]. Researchers continue to explore diverse glass compositions to optimize performance for temperature measurement systems [8–13]. Among the various glass families investigated, tellurite-based compositions have garnered significant attention due to their outstanding material properties. These include manageable melting temperatures, excellent capacity to accommodate lanthanide ions, robust thermal and chemical stability, superior infrared transmissivity, high dielectric constants, minimal optical losses, elevated refractive indices, and favorable phonon energies [14–17].Tellurite dioxide (TeO_2) serves as the foundational glass former, but its glass-forming ability improves

ISSN 2278-2540 | DOI: 10.51583/IJLTEMAS | Volume XV, Issue VII, July 2026

substantially when combined with modifier oxides. The incorporation of tungsten oxide (WO_3) as a network modifier strengthens the glass framework, enhances thermal and chemical durability, and permits compositional flexibility across multiple components [18]. Additionally, WO_3 contributes its own benefits—namely strong optical transparency and high refractive index stability [19]. The introduction of alkali oxides such as sodium oxide (Na_2O) further refines these materials by improving thermal stability, creating non-bridging oxygen sites, and enhancing ionic mobility factors that collectively increase the capacity to dissolve lanthanide ions within the glass matrix [20].This investigation presents a comprehensive analysis of the physical and optical properties of Ho^{3+}-doped tellurite glass, with particular emphasis on upconversion phenomena. By examining the distinctive emission bands present in upconverted photoluminescence spectra across prepared samples, we aim to demonstrate the viability of these materials for display and sensing device applications.

Glass synthesis

The holmium-doped tungsten tellurite glass samples were prepared according to the following molar composition: $(70-x)\%\ TeO_2 - 10\%\ Na_2O - 20\%\ WO_3 - x\%\ Ho_2O_3$where the holmium content (x) was set at 0.5, 1.0, or 1.5 mol%, and the corresponding samples were designated as TNWH1 , TNWH2 and TNWH3, respectively. For each batch, precisely weighed raw materials totaling 15 grams were thoroughly mixed and then melted inside a covered alumina crucible at 950 ℃ for 45 minuts. To ensure compositional uniformity, the molten mixture was stirred manually at regular intervals throughout the melting process. The homogenized melt was rapidly cooled by pouring it into a stainless steel mold to form solid glass samples. These as-quenched samples were then transferred to an annealing furnace, where they were heated to 320℃ and held at that temperature for 1.5 hours. This annealing step allowed any residual internal stresses—introduced during the rapid quenching process—to gradually relax. Finally, the samples were cooled down slowly inside the furnace to room temperature. The resulting glass specimens, shaped as pellets, were carefully polished on both sides to obtain smooth, plane-parallel surfaces suitable for subsequent optical and physical characterizations.

Measurements and characterization studies

The amorphous nature of the glass samples was confirmed through X-ray diffraction (XRD) analysis, carried out at room temperature on a Rigaku SmartLab 9kW diffractometer over a 2θ range of 10°–80°, as shown in Fig. 1. The patterns for all three samples (TNWH1, TNWH2, and TNWH3) show only broad, diffuse humps rather than sharp, well-defined peaks. This absence of sharp diffraction peaks is the classic signature of a disordered, non-crystalline glassy network, confirming that the samples retained their amorphous structure.

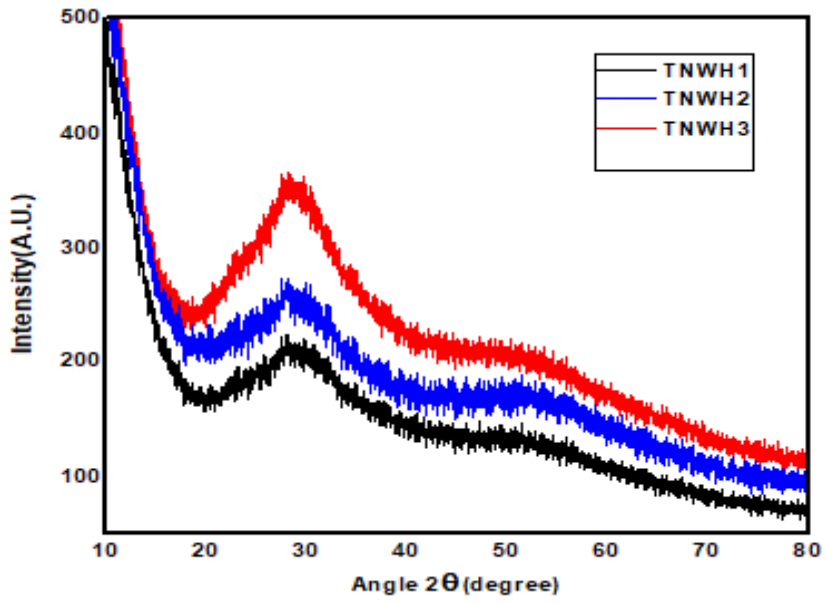

Fig.1. X-Ray diffractgram of TNWH glasses

ISSN 2278-2540 | DOI: 10.51583/IJLTEMAS | Volume XV, Issue VII, July 2026

The thermal behavior of the glass samples was investigated using differential scanning calorimetry (DSC) on a TA Instruments Q10 (USA), operating at a heating rate of 10 °C/min, with the resulting thermogram presented in Fig. 2. The glass transition temperature (Tg) was identified from the characteristic endothermic inflection in the calorimetric curve, where the signal shifts from its initial baseline, corresponding to the change in heat capacity as the glass network transitions from a rigid to a more flexible, supercooled state. For the TNWH2 sample, this transition was observed at Tg = 310 °C. Upon further heating, a sharp exothermic rise appeared at higher temperatures, marking the onset of crystallization; this crystallization temperature (Tc) was recorded at 500 °C. The relatively wide thermal stability window between Tg and Tc ($\Delta T = Tc - Tg = 190$ °C) suggests good resistance to devitrification, indicating that the glass can be thermally processed over a broad temperature range without a high risk of unwanted crystallization.

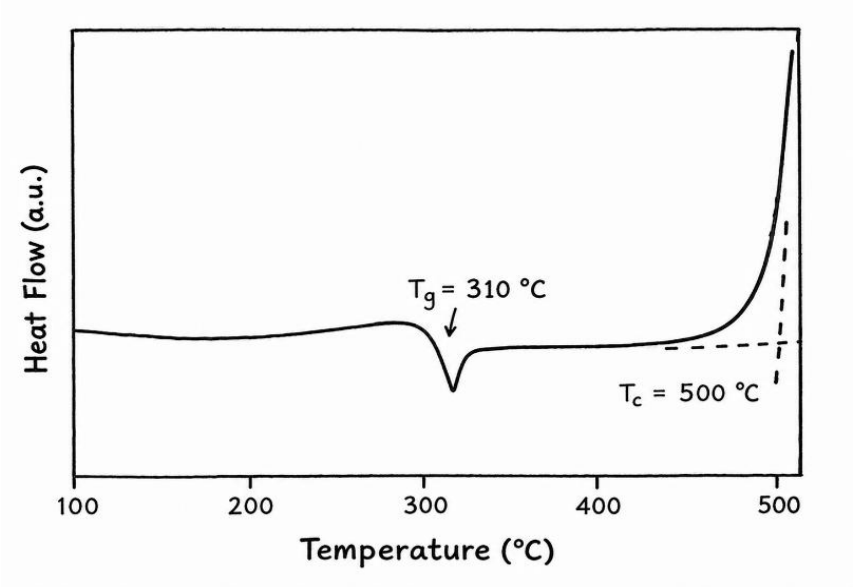

Fig.2. DSC plot of TNWH2 sample

Physical properties

The physical properties of glassy materials play a vital role in understanding their optical behavior, and among these, density and refractive index are especially important because they influence parameters such as average molecular weight, mean atomic volume, and related structural features. The evaluated physical properties of the TNWH glass series are summarized in Table 1, which also shows how density and refractive index vary with Ho^{3+} concentration. It is observed that the density of the synthesized glasses gradually increases as the Ho^{3+} content rises. This increase in density suggests a more compact glass network, likely due to the incorporation of additional bridging oxygen bonds, which in turn makes the glass structure more rigid. The variation in Ho^{3+} ion concentration also affects the average molecular weight and interatomic distance of the glasses. Using pure water as the immersion medium and a high-sensitivity electronic balance for density measurement, it was found that the average molecular weight increases while the interatomic distance decreases with increasing Ho^{3+} content. In addition, other important physical parameters such as molar mass, molar volume, lanthanide ion concentration, polaron radius, interionic distance, field strength, and oxygen packing density were also calculated [21].

Table1. Physical Parameters of TNWH Glasses

S.No.	Physical Properties	TNWH1	TNWH2	TNWH3
1	Composition TeO_2:Na_2O:WO_3:Ho_2O_3	69.5:10:20:0.5	69:10:20:01	68.5:10:20:1.5
2	Density (d) (g/cm^3)	5.011	5.014	5.016

ISSN 2278-2540 | DOI: 10.51583/IJLTEMAS | Volume XV, Issue VII, July 2026

3	Mol. Mass(mole)	165.68	166.78	167.78
4	Mol. volume(cm^3/mol)	31.375	31.319	31.196
5	Lanthanide ion concentration(c_L) ($c_L \times 10^{20}$) (ions/cm^3)	1.797	3.583	5.342
6	Polaron radius (p_r)(Å)	4.95	3.933	3.44
7	Inter ionic distance (I_r)(Å)	17.718	14.078	12.324
8	Field strength ($F_L \times 10^{13}$) (cm^2)	9.556	15.135	19.752
9	Oxygen Packing Density (OPD) (g-atom/l)	63.664	63.434	63.201

Optical absorption

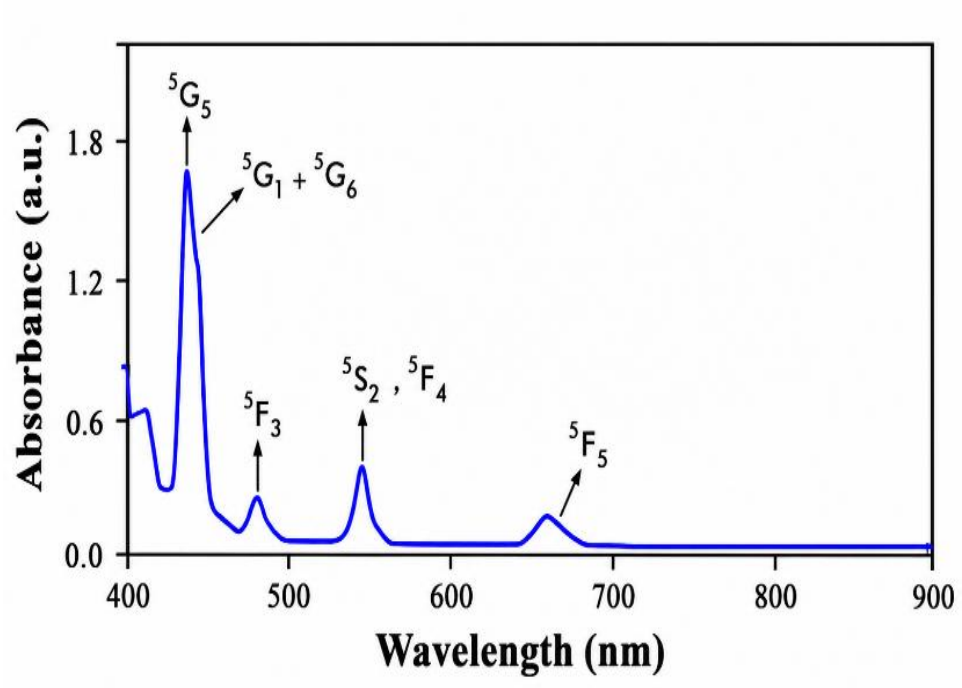

Fig. 3. Absorption spectra of TNWH2 sample

The optical absorption spectra of the prepared TNWH glass samples in the visible-near infrared (Vis-NIR) region are presented in Figure 3. Analysis of these spectra revealed a rich pattern of absorption features characteristic of Ho^{3+} doping. A total of seven distinct absorption peaks were identified, each corresponding to specific electronic transitions of Ho^{3+} ions from their ground state $^5I_8$ to various higher-energy excited states. The absorption peaks, centered at wavelengths of 419, 451, 485, 539, 643, and 1154 nm, were assigned to transitions from the ground state $^5I_8$ to the excited states $^5G_5$, $^5G_6$, $^5F_3$, $^5F_{4+}$, $^5S_2$, $^5F_5$, and $^5I_6$, respectively. This complex multiplet structure arises from the intrinsic energy level manifold of the Ho^{3+} ion, which contains numerous closely spaced electronic states. The presence of multiple absorption bands across a broad spectral range demonstrates the versatility of Ho^{3+} as an active dopant for optical applications. The rich energy level structure of Ho^{3+} ions makes them particularly attractive for a wide variety of photonic and optoelectronic device applications, including laser systems, amplifiers, and wavelength-selective optical components, where precise control over light absorption and emission is essential.

ISSN 2278-2540 | DOI: 10.51583/IJLTEMAS | Volume XV, Issue VII, July 2026

Upconversion in Ho3+-doped TNW glasses

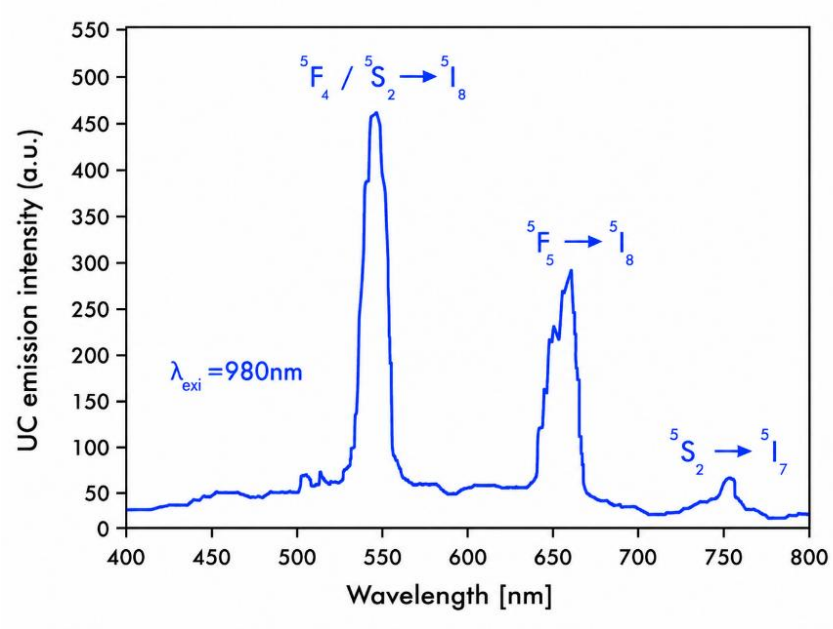

Fig. 4. Emission spectra of TNWH2 sample

The optical absorption spectra of the prepared TNWH glass samples in the visible-near infrared (Vis-NIR) region are presented in Figure 3. Analysis of these spectra revealed a rich pattern of absorption features characteristic of Ho^{3+} doping. A total of seven distinct absorption peaks were identified, each corresponding to specific electronic transitions of Ho^{3+} ions from their ground state $^5I_8$ to various higher-energy excited states. The absorption peaks, centered at wavelengths of 419, 451, 485, 539, 643, and 1154 nm, were assigned to transitions from the ground state $^5I_8$ to the excited states $^5G_5$, $^5G_6$, $^5F_3$, $^5F_{4+}$, $^5S_2$, $^5F_5$, and $^5I_6$, respectively. This complex multiplet structure arises from the intrinsic energy level manifold of the Ho^{3+} ion, which contains numerous closely spaced electronic states. The presence of multiple absorption bands across a broad spectral range demonstrates the versatility of Ho^{3+} as an active dopant for optical applications. The rich energy level structure of Ho^{3+} ions makes them particularly attractive for a wide variety of photonic and optoelectronic device applications, including laser systems, amplifiers, and wavelength-selective optical components, where precise control over light absorption and emission is essential.

Transition Mechanism

The observed upconversion emissions in the TNWH glass samples can arise through several distinct physical mechanisms, each involving the sequential absorption of multiple photons and subsequent relaxation pathways. The primary mechanisms responsible for the recorded upconversion luminescence include: (a) two-photon absorption combined with multiphonon relaxation, (b) phonon-assisted two-photon absorption, and (c) cross-relaxation (CR) coupled with excited-state absorption (ESA) processes that facilitate effective two-photon absorption.

The population of the thermally coupled excited states $^5F_4$ and $^5S_2$, as well as the higher-energy level $^3K_8$ and $^5F_3$, occurs sequentially through the absorption of two 980 nm photons by ground-state absorption (GSA), excited-state absorption (ESA), and phonon-assisted relaxation processes. Once populated in these elevated energy states, excited Ho^{3+} ions undergo nonradiative relaxation, cascading downward to the thermally coupled $^5F_4/^5S_2$ levels. From these intermediate states, the ions then radiatively de-excite to the ground state $^5I_8$ through the $^5F_4/^5S_2 \rightarrow {}^5I_8$ transition, producing green emission at 547 nm. Similarly, the $^5F_5 \rightarrow {}^5I_8$ transition generates red emission at 660 nm, and the $^5S_2 \rightarrow {}^5I_7$ transition produces near-infrared emission at 760 nm.

An important observation regarding the spectral distribution of upconversion emission is that under conditions of reduced excitation power, red emission dominates over green emission. This phenomenon arises from

ISSN 2278-2540 | DOI: 10.51583/IJLTEMAS | Volume XV, Issue VII, July 2026

resonant cross-relaxation processes occurring between pairs of Ho^{3+} ions. When two adjacent Ho^{3+} ions interact through the $^3K_8$; $^5I_8 \rightarrow {}^5F_5$; $^5I_7$ cross-relaxation transition, one ion is excited while its neighbor relaxes to a lower state, effectively transferring energy within the ion pair. This process populates the $^5I_7$ level, which then absorbs a second 980 nm photon via the ESA mechanism to populate $^5F_5$. From this state, a direct radiative transition to the ground level produces the characteristic red fluorescence at approximately 660 nm. The efficiency of the cross-relaxation process is critically dependent on both the concentration of Ho^{3+} dopant ions and the interionic distance within the host glass matrix. Higher dopant concentrations and shorter interionic separations—achieved through increased Ho^{3+} loading or modification of the host matrix composition—enhance the probability of cross-relaxation interactions, thereby promoting preferential red emission at lower pump powers. Conversely, at elevated excitation powers, direct multiphoton pathways become more competitive, resulting in enhanced population of the green-emitting $^5F_4/^5S_2$ states and a corresponding increase in overall upconversion brightness [24, 25, 26].

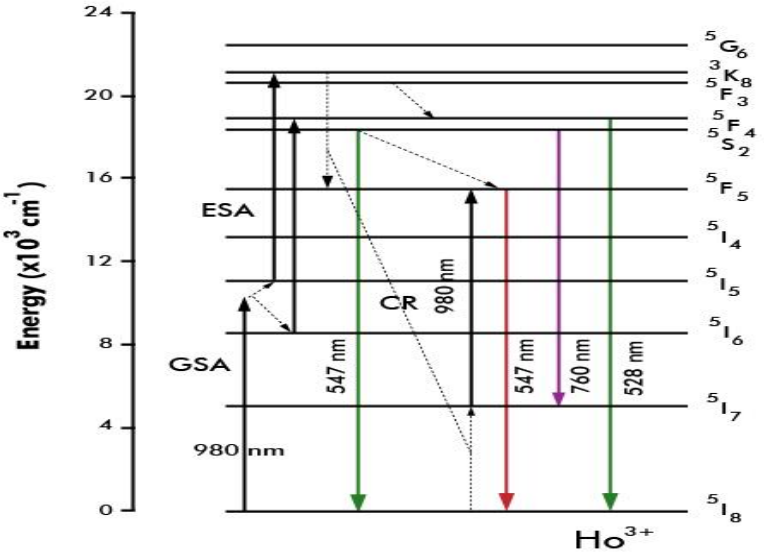

Fig.5. Mechanism of upconversion

CONCLUSION

Non-crystalline Ho^{3+}-activated TeO_2-Na_2O-WO_3 glasses were successfully synthesized using the conventional melt-quenching technique, demonstrating efficient upconversion luminescence with bright green and red emission under near-infrared excitation. Thermal characterization of the prepared glasses, performed via differential scanning calorimetry (DSC), revealed a glass transition temperature (Tg) of 310°C and a crystallization temperature (Tc) of 500°C. These thermal parameters define the stability window of the glassy phase and indicate favorable thermal properties for device fabrication and processing without unwanted crystallization. Optical absorption spectroscopy identified six prominent absorption peaks centered at wavelengths of 419, 451, 485, 539, 643, and 1154 nm, corresponding to electronic transitions of Ho^{3+} ions from the ground state to various excited energy levels. Upon excitation with 980 nm laser radiation, the Ho^{3+}-doped glasses exhibited efficient upconversion luminescence, generating detectable photons in the visible spectrum through multiphoton absorption mechanisms. A particularly notable feature of the upconversion process was the observation of tunable color emission, with the spectral output varying from yellow to green to red across a range of excitation conditions or dopant concentrations. This color tunability arises from the variable population of different excited states as a function of excitation power and Ho^{3+} ion interactions within the glass matrix. The ability to produce bright, tunable visible emission from near-infrared pump radiation demonstrates the potential of these Ho^{3+}-activated tellurite glasses for advanced photonic applications including tunable light sources, display technologies, biomedical imaging, and other wavelength-selective optical devices.

ISSN 2278-2540 | DOI: 10.51583/IJLTEMAS | Volume XV, Issue VII, July 2026

REFERENCES

1. X. Zhang, J. Wang, L. Huang, F. Pan, Y. Chen, B. Lei, ACS Appl. Mater. Interfaces 7 (2015) 10044–10054.
2. J.L. Liu, Y.B. Xiao, S.J. Huang, L.Y. Mao, W.C. Wang, Q.Y. Zhang, , J. Non. Solids 522 (2019), 119564.
3. M. Haouari, A. Maaoui, N. Saad, A. Bulou, A Phys. 261 (2017) 235–242.
4. S. Hashim, M.H.A. Mhareb, S.K. Ghoshal, Y.S.M. Alajerami, D.A. Bradley, M.I. Saripan, et al., Radiat. Phys. Chem. 116 (2015) 138–141.
5. O. Kibrisli, N. Vahedigharehchopogh, A.E. Ersundu, M. Celikbilek Ersundu, J. Phys. Chem. C (2020).
6. N. Vahedigharehchopogh, O. Kıbrıslı, A.E. Ersundu, M. C¸ elikbilek Ersundu, J. Non. Solids 525 (2019), 119679.
7. O. Kıbrıslı, A.E. Ersundu, , Appl. Phys. A 124 (2018) 375.
8. L. Shamshad, G. Rooh, K. Kirdsiri, N. Srisittipokakun, H.J. Kim, J. Kaewkhao, J. Mol. Struct. 1125 (2016) 601–608.
9. G.C. Ram, T. Narendrudu, S. Suresh, A.S. Kumar, M.V.S. Rao, V.R. Kumar, et al., Opt. Mater. 66 (2017) 189–196.
10. F. Zaman, J. Kaewkhao, N. Srisittipokakun, N. Wantana, H.J. Kim, G. Rooh, Opt. Mater. 55 (2016) 136–144.
11. Z. Liu, H. Deng, D. Chen, Ceram. Int. 45 (2019) 13235–13241.
12. F. Huang, Y. Gao, J. Zhou, J. Xu, Y. Wang, J. Alloys. Compd. 639 (2015) 325–329.
13. L. Li, F. Qin, Y. Zhou, Y. Zheng, H. Zhao, Z. Zhang, J. Lumin. 202 (2018) 301–308.
14. M. C¸ elikbilek Ersundu, A.E. Ersundu, J. Non. Solids 453 (2016) 150–157.
15. A.E. Ersundu, M. C¸ elikbilek, N. Solak, S. Aydin, J. Eur. Ceram. Soc. 31 (2011) 2775–2781.
16. A.E. Ersundu, G. Karaduman, M. Elikbilek, N. Solak, S. Aydin, J. Alloys. Compd. 508 (2010) 266–272.
17. E. Erol, O. Kıbrıslı, M. C¸ elikbilek Ersundu, A.E. Ersundu, Chem. Eng. J. 401 (2020), 126053.
18. A.E. Ersundu, M. C¸ elikbilek, S. Aydin, J. Non. Solids 358 (2012) 641–647.
19. H. Kumari , K. Patel , S.K. Dhiman , S.K. Mahajan , G. F. Ansari, Materials Today: Proceedings, 2022 Volume 59, Part 1, 2022, Pages 1127-1131,
20. M. C¸ elikbilek, A.E. Ersundu, E.O. Zayim, S. Aydin, J. Alloys. Compd. 637 (2015) 162–170.
21. G.F. Ansari, R.P. Kumbhakar, R.P, ,S.K. Dhiman, S. K. Mahajan,, 2022. Materials Today: Proceedings, 56, pp.1313-1316.21.
22. S. Balaji, A. D. Sontakke, R. Sen, A. Kalyandurg, Opt. Mater. Express, 1 (2011) 138-150.
23. H. M. Crosswhite, H. Crosswhite, N. Edelstein, K. Rajnak, J. Chem. Phys., 67 (1977) 3002-3010
24. A. Pandey, and V. K. Rai, Dalton Trans., 42 (2013) 11005-11011.
25. Y. Dwivedi, A. Bahadur, S. B. Rai, J. Appl. Physics, 110 (2011) 043103
26. A. S. Gouveia-Neto, E. B. da Costa, L. A. Bueno, S. J. L. Ribeiro, J. Lumin., 110 (2004) 79-84